the FEBS Journal

# Post-translational cleavage of recombinantly expressed nitrilase from *Rhodococcus rhodochrous* J1 yields a stable, active helical form

R. Ndoria Thuku[1,2], Brandon W. Weber[2], Arvind Varsani[2] and B. Trevor Sewell[1,2]

1 Department of Biotechnology, University of the Western Cape, Bellville, South Africa
2 Electron Microscope Unit, University of Cape Town, Rondebosch, South Africa

**Keywords**
electron microscopy; helix; IHRSR; nitrilase; oligomeric form

**Correspondence**
B. T. Sewell, Electron Microscope Unit, University of Cape Town, Private Bag, Rondebosch 7701, South Africa
Fax: +272 168 91528
Tel: +272 165 02817
E-mail: sewell@uctvms.uct.ac.za

(Received 23 January 2007, revised 14 February 2007, accepted 20 February 2007)

doi:10.1111/j.1742-4658.2007.05752.x

Nitrilases convert nitriles to the corresponding carboxylic acids and ammonia. The nitrilase from *Rhodococcus rhodochrous* J1 is known to be inactive as a dimer but to become active on oligomerization. The recombinant enzyme undergoes post-translational cleavage at approximately residue 327, resulting in the formation of active, helical homo-oligomers. Determining the 3D structure of these helices using electron microscopy, followed by fitting the stain envelope with a model based on homology with other members of the nitrilase superfamily, enables the interacting surfaces to be identified. This also suggests that the reason for formation of the helices is related to the removal of steric hindrance arising from the 39 C-terminal amino acids from the wild-type protein. The helical form can be generated by expressing only residues 1–327.

Nitrilases are useful industrial enzymes that convert nitriles to the corresponding carboxylic acids and ammonia. They belong to a superfamily [1] that includes amidases, acyl transferases and *N*-carbamoyl-D-amino acid amidohydrolases, and they occur in both prokaryotes and eukaryotes. Their applications include the manufacture of nicotinic acid, ibuprofen and acrylic acid and the detoxification of cyanide waste [2,3]. Although nitrilases hydrolyse a variety of nitriles, their natural substrates are, in general, not known. Environmental sampling and sequence analysis has substantially increased our knowledge of the distribution and specificity of these enzymes [4,5], but detailed structural information on nitrilases, which would enable a correlation between sequence and specificity, is not yet available.

Members of this superfamily have a characteristic αββα-fold, a conserved Glu, Lys, Cys catalytic triad and divergent N- and C-termini. The atomic structures of five homologous enzymes in the superfamily are known, namely the Nit domain of NitFhit fusion protein (1ems) [6], the *N*-carbamoyl-D-amino acid amidohydrolase (1erz, 1uf5) [7,8], the putative CN hydrolase from yeast (1f89) [9], the hypothetical protein PH0642 from *Pyrococcus horikoshii* (1j31) [10] and the amidase from *Geobacillus pallidus* RAPc8 [11]. All the structures are distant homologues having slightly $> 20\%$ identity. All have a twofold symmetry that conserves interactions between two helices at the subunit interface known as the A surface [12] (see supplementary Fig. S3). This leads to an extended αββα–αββα-fold. Although these nitrilase homologues exist as dimers or tetramers, microbial nitrilases occur as higher homo-oligomers [3].

Only in the case of the cyanide dihydratases [13,14] is there any information about the quaternary structure of the microbial nitrilases. The *Pseudomonas stutzeri* enzyme is an unusual, 14-subunit, self-terminating, homo-oligomeric spiral, whereas that from *Bacillus pumilus* shows reversible, pH-dependent, switching between an 18-subunit, self-terminating, spiral form and a variable-length, regular helix. Docking a homology model into the 3D reconstruction of the negative stain envelope of the cyanide dihydratase of

*P. stutzeri* led to the identification of four regions in which the subunits interact to form the spiral – the A, C, D and E surfaces [12]. The A surface has been described above. The C surface is located almost at right angles to the A surface and leads to elongation of the spiral. Two sequence insertions relative to the crystallographically determined homologues are correctly positioned to contribute to this interface. The D surface comprises interactions across the groove which can occur only after the spiral has completed a full turn. In the case of *P. stutzeri* cyanide dihydratase, an additional set of interactions across the groove at the E surface leads to termination of the spiral.

*Rhodococcus rhodochrous* J1 nitrilase is known to form higher oligomers and acquire activity in response to benzonitrile, heat treatment and ammonium sulfate [15,16]. Activation of the enzyme on oligomerization of the dimers is typical of Rhodococcal nitrilases [17,18], and links formation of the quaternary structure to the activity. Knowledge of interactions stabilizing the quaternary structure may lead to an understanding of the oligomerization-dependent activation and may enable control of their oligomeric state in the industrial situation. Here, we report the discovery of a specific post-translational cleavage of recombinantly expressed nitrilase from *R. rhodochrous* J1 which leads to the formation of stable, active helices. 3D reconstruction of the negatively stained fibres, followed by docking a homology model into the density, both confirms the general principles observed in the case of the cyanide dihydratases, and also leads to definite suggestions about the interacting residues. Examination of the complexes formed prior to post-translational cleavage suggests that steric hindrance resulting from the C-terminal 39 amino acids causes failure of the interactions leading to helix formation.

## Results

Freshly prepared, full-length recombinant enzyme (expressed in *Escherichia coli*) was separated by gel-filtration chromatography into fractions containing an active 480-kDa oligomer and an inactive 80-kDa dimer, both composed of the same 40-kDa polypeptide

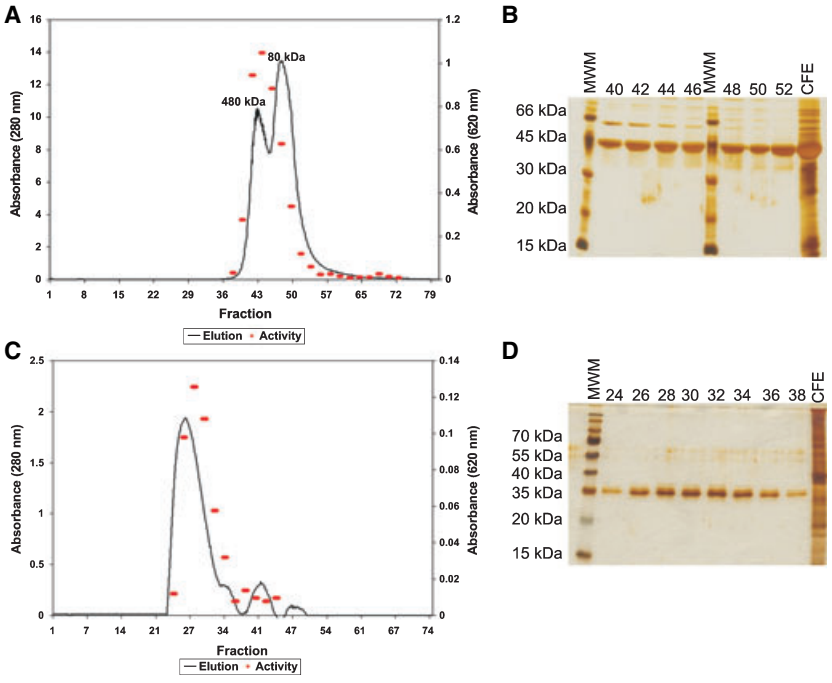


**Fig. 1.** Gel-filtration chromatography of the recombinant nitrilase from *R. rhodochrous* J1. (A) Elution of the active 480-kDa oligomer and the inactive 80-kDa dimer in 100 mM $KH_2PO_4$, 200 mM NaCl, pH 7.8 using a Sephacryl S400 HR column. Solid line, protein concentration measured by $D_{280}$; red bars, activity measured by $D_{620}$ according to our assay. Note that the left-hand point of the bar indicates the fraction assayed. (B) Reducing SDS/PAGE of the active fraction showed a characteristic nitrilase band of ~40 kDa. The contaminating band at 60 kDa was identified as GroEL on the basis of its characteristic appearance in the micrographs. CFE, cell-free extract; MWM, molecular mass marker. (C) Elution of a 1-month-old active fraction in 100 mM $KH_2PO_4$, 200 mM NaCl, pH 7.8 using a TSK G5000PW$_{XL}$ column. The molecular mass was > 1.5 MDa. (D) Reducing SDS/PAGE showed a distinct band of subunit atomic mass 36.5 (± 0.6) kDa. The two columns used in (A) and (C) have very similar separation characteristics. The elution profiles have been scaled so that the 80 and 480 kDa elution positions coincide.

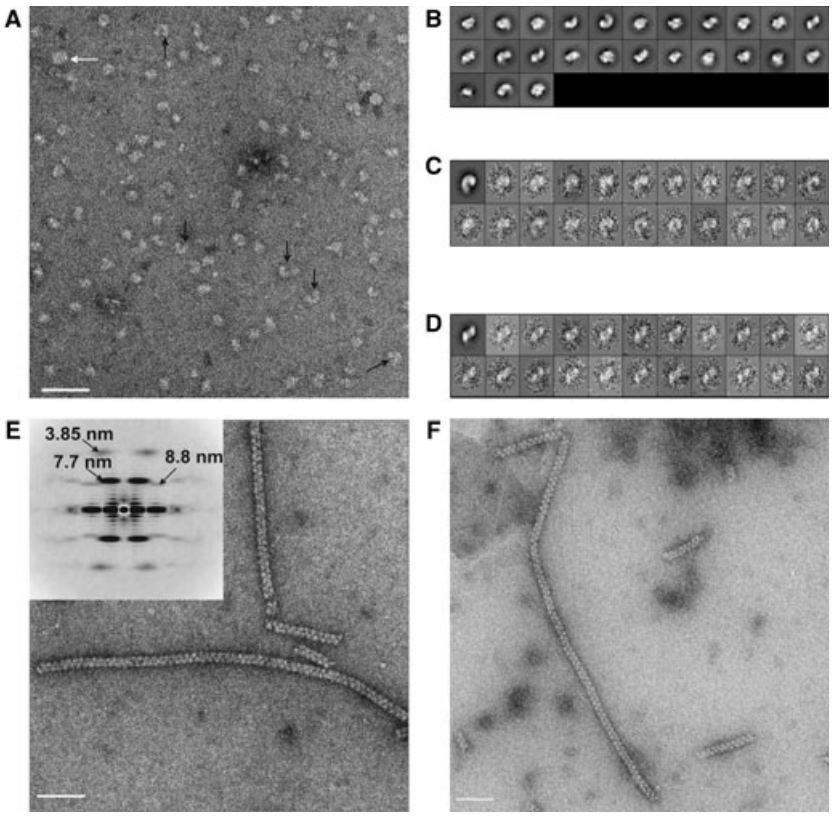


**Fig. 2.** Low-dose electron micrographs of purified and active recombinant nitrilase of *R. rhodochrous* J1. (A) Quaternary polymorphism of the 480 kDa oligomer. 'C'-shaped particles (black arrows) and occasional GroEL contamination (white arrow) can be seen. (B) Twenty-five class averages representing common particle views generated by iterative alignment, sorting and classification of isolated particle images. (C, D) Putative top and side views of 'c'-shaped class members and the corresponding class average are shown. The length of the 'c' varied between 9 and 13 nm. (E) Helices formed after storage of the recombinant wild-type nitrilase at 4 °C for 1 month. A power spectrum of the filament structure (insert) shows a strong layer line, indexed as a Bessel function of order −1, corresponding to a helix with a pitch of 7.7 nm. The layer line at 8.8 nm has been indexed as being a fourth-order Bessel function. The diameter of the helix is 13 nm. (F) Helices formed from the expression product of J1ΔC327 which is truncated after residue 327 are indistinguishable from those in (E). White scale bar = 50 nm.

chain (Fig. 1A,B). Even though the protein runs as a single characteristic band on SDS/PAGE, negative-stain electron microscopy shows an apparently heterogeneous mixture of particles of different shapes and sizes (Fig. 2A,B). Classification, alignment and averaging of the particles confirms the heterogeneity and, in addition, demonstrates the existence of a significant subset of particles that resemble the letter 'c' viewed from different angles (Fig. 2C,D).

After storage at 4 °C for 1 month, the active fraction eluted from the gel-filtration column in the void volume indicating a mass > 1.5 MDa (Fig. 1C and supplementary Fig. S1). Reducing SDS/PAGE showed that the subunit atomic mass was 36.5 (± 0.6) kDa (Fig. 1D). This was confirmed by MS analysis, which gave a sharp peak at 36 082 Da (R.L. Wolz, Commonwealth Biotechnologies Inc., Richmond, VA). N-Terminal sequencing confirmed that the N-terminal was intact and that C-terminal residues had been removed. The sharpness of the band on the polyacrylamide gel suggests that this is due to specific cleavage. The calculated masses of fragments 1–326 and 1–327 are 35 990 and 36 127 Da, respectively, indicating the loss of ~39 amino acids from the C-terminus. Using negative-stain electron microscopy, the fraction was shown to contain a homogeneous helical form (Fig. 2E). Analysis of these helices showed that they had a diameter of 13 nm, a pitch of 7.7 nm and were of variable length.

3D reconstruction of the fibres using the iterative, real-space method of Egelman [19] showed that the helices had 4.9 dimers per turn of the helix, in which each dimer has an azimuthal rotation of −73.65° and an axial rise of 1.58 nm (convergence is shown in supplementary Fig. S2). This corresponds to 78 dimers

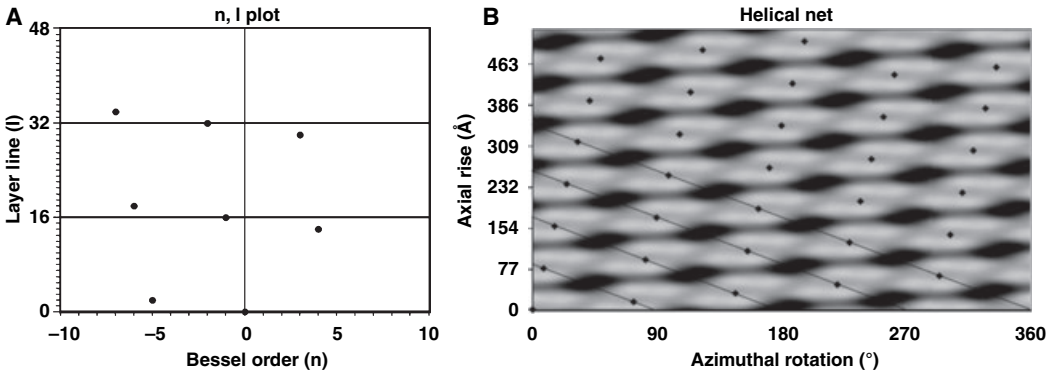


**Fig. 3.** (A) An n,l plot which enables indexing of the power spectrum shown as the insert to Fig. 2E based on there being 78 dimers in 16 turns. (B) A helical net superimposed on the projected density of the reconstructed map viewed from the inside. In this representation the left-handed one-start helices run from lower left to top right. The set of right-handed four-start helices are indicated by the lines running from top left to bottom right. The symmetry of the helix can be described as $D_1S_{4.9}$ following the notation of Makowski & Caspar [33].

in 16 turns and enables indexing of the power spectrum (Fig. 2E, insert) as shown in Fig. 3A. The clear diffraction spot with a spacing of 7.7 nm is interpreted as a Bessel function of order −1, corresponding to the set of left-handed, one-start helices depicted in the helical net (Fig. 3B). The diffraction spot with a spacing of 8.8 nm is interpreted as being a Bessel function of order +4, corresponding to the set of right-handed, four-start helices depicted in the helical net. It would be consistent to interpret the diffraction spot with a spacing of 3.85 nm as corresponding to the unseparated Bessel functions of orders −2 and +3.

The volume of density containing each subunit can be clearly discerned. Connections along the one-start helix occur at two intermolecular interfaces designated the A and C surfaces, respectively (Fig. 4). The one-start helix is further stabilized by an interaction across the groove at the D surface. There are two clearly defined dyad axes perpendicular to the helix axis. One passes through the C and D surfaces on opposite sides of the helix and the other passes through the A surface and a prominent hole on the other side of the helix. The helix has many features in common with the *P. stutzeri* and *B. pumilus* cyanide dihydratase spirals [13,14]. Long helices of the *B. pumilus* cyanide dihydratase have been shown by shadowing to be left-handed. This handedness is consistent with the modelling and docking described here.

Further interpretation of the map required the creation of a model of the J1 nitrilase based on its homology with members of the superfamily for which crystal structures exist (Fig. 6). Alignment of the sequence against those homologues using MGENTHREADER [20] showed that the enzyme has two significant insertions (residues 54–73 and 234–247) and an extended C-terminus relative to these enzymes (Figs 5,6). These insertions have previously been proposed to associate in the spiral oligomer of the cyanide dihydratase to form the C surface [16], which leads to spiral elongation.

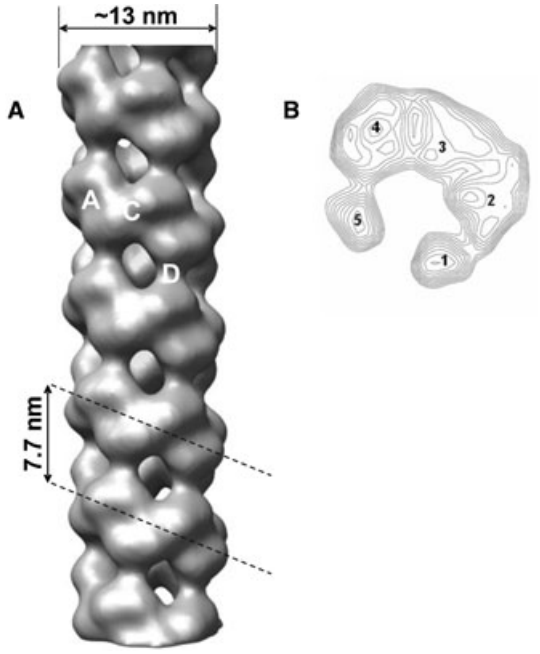


**Fig. 4.** The 3D reconstruction of the stain envelope of the C-terminal truncated nitrilase from *R. rhodochrous* J1. (A) Interactions between the subunits occur at the surfaces marked A, C and D. The A surface is preserved in all members of the nitrilase superfamily whose structures have been determined crystallographically and can be identified from the shape of the molecule. (B) A contoured cross-section of the map (0.4 nm thick) shows the subunit boundaries and a central core which is vacant. The numbers 1–5 indicate regions in the contoured sections corresponding to different dimers.

**Fig. 5.** Multiple sequence alignment of the nitrilase from *R. rhodochrous* J1 (RrJ1) with four nitrilase homologues for which the crystal structures are known, namely 1ems [6], 1erz [7], 1f89 [9] and 1j31 [10]. Two significant insertions in its sequence (corresponding to residues 54–73 and 234–247) relative to the solved structures are located at the C surface. Furthermore, none of these homologues suggests a model for the structure of the C-terminal region. The conserved active-site residues are outlined, conserved or homologous residues are in italics and double underlines indicate the position or the residues which were mutated to stop codons (Table 1). The approximate regions of interacting surfaces A, C and D are indicated on the top line. Charged residues which are possibly involved in interactions at the D surface are indicated in bold and the external loop regions are shaded grey. The secondary structural elements identified in 1erz [7] are indicated in the bottom line.

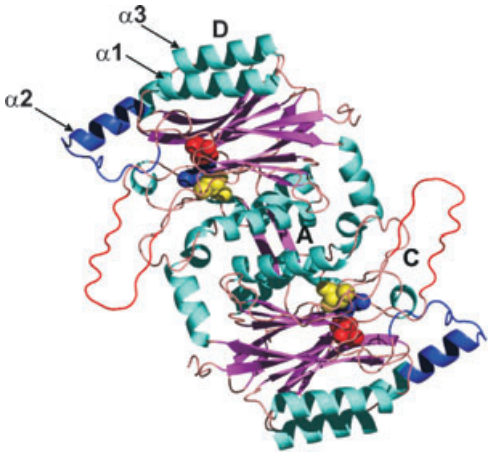


**Fig. 6.** *R. rhodochorus* J1 nitrilase model based on the solved structure. There are two significant insertions in its sequence, relative to the homologues, namely residues 54–73 (blue) and 234–247 (red). The catalytic residues, Glu48 (red), Lys131 (blue) and Cys165 (yellow) are illustrated as spheres. The positions of the structural elements referred to in the text are indicated.

The strong conservation of the fold, which preserves all but the peripheral loops, makes it possible to build a plausible model of the J1 nitrilase which, in turn, makes it possible to interpret the stain envelope.

At 1.8 nm resolution, the shape of the homologues (Fig. 7) can be readily discerned in the reconstruction of the stain envelope. The A surface clearly corresponds to the dimer interface conserved in all the homologues. Docking of the model [21] (see Experimental procedures) into the stain envelope is simplified because the symmetry restricts the number of degrees of freedom. The twofold axis of the dimer model must coincide with the appropriate twofold axis of the stain envelope. Thus, the two possible degrees of freedom (apart from the known helical parameters) are the radial distance of the model along the dyad axis and the rotation about the dyad axis. Our docking procedure, which utilized these constraints, produced an unambiguous optimal fit to the stain envelope.

Four important insights emerge from the docking (Fig. 7). The C-terminal region is located on the inside of the helix adjacent to the central channel. There is some vacant density in this region which may accommodate residues 314–327. There is also sufficient vacant density between the subunits in the C surface region to accommodate the insertions that have not been modelled (residues 54–73 and 234–247). The docking places the bend between beta-sheets β3 and β4 (residue 108) in close proximity to alpha-helix α7 (residue 289) suggesting the possibility of an interaction in this region which contributes to stabilizing the C surface. The D surface is formed by symmetric interactions that occur in the helix α3 having the sequence -RLLDAARD-. The presence of two arginine and two

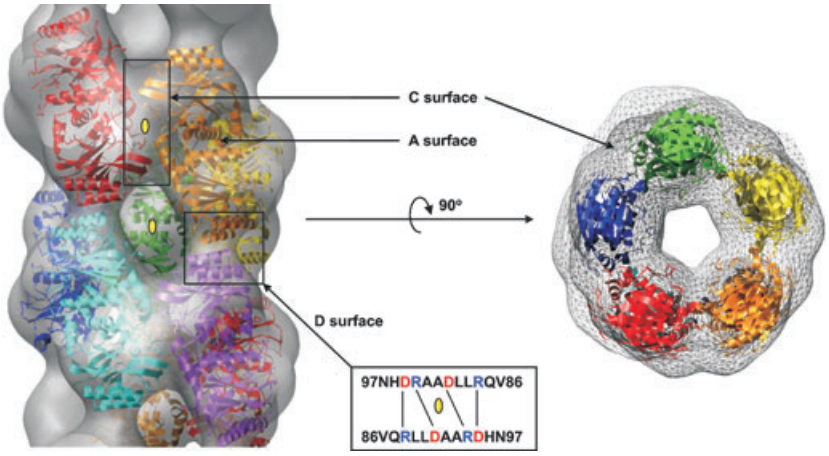


**Fig. 7.** Fitting of *R. rhodochrous* J1 nitrilase models into the 3D stain envelope. The helix is built from dimers formed across the A surface, which interact via the C and D surfaces. There is a possibility of four symmetric salt bridges between helices (corresponding to α3 in 1erz) [7] located at the D surface (box outline). Regions of vacant density at the C surface correspond to the location of insertions that are not modelled. There are two horizontal dyads (yellow ellipses), one located at the A surface passing through the hole on the other side of the helix and the other at the D surface passing through the C surface on the other side of the helix.

aspartic acid residues suggests that up to four ion pairs may be formed in this region.

It is necessary to explain why the full-length enzyme failed to form extended helices. Certainly the prominence of 'c'-shaped aggregates (Fig. 2B–D) is suggestive of a tendency towards helix formation. Based on our observation that the C-terminus is located in the centre of the helix we suggest that, in the case of the full-length enzyme, steric hindrance results in a spiral of a non-optimal diameter, in which D surface interactions cannot occur. Thus, the extended helix cannot be stabilized. To test this hypothesis a series of mutant enzymes were prepared in which stop codons were inserted after positions 302, 311, 317, 327, and 340 (Table 1). Short helical segments, as well as the 'c'-shaped particles, were seen in both the J1ΔC317 and J1ΔC340 mutants (results not shown), but the J1ΔC327 mutant produced long helices indistinguishable from those found to occur naturally (Fig. 2F). Both the J1ΔC302 and J1ΔC311 mutants were inactive, indicating that some interaction essential for helix formation (and hence activity) [12] was lost by truncating the enzyme to this extent. These mutants were not explored further.

**Table 1.** Mutations of the nitrilase from *R. rhodochrous* J1.

| Name | Description | Substitution | Activity |
|---|---|---|---|
| J1ΔC302 | C-terminal truncation | V303stop | Inactive |
| J1ΔC311 | C-terminal truncation | H312stop | Inactive |
| J1ΔC317 | C-terminal truncation | T318stop | Active |
| J1ΔC327 | C-terminal truncation | T328stop | Active |
| J1ΔC340 | C-terminal truncation | E341stop | Active |

## Discussion

The nitrilase from *R. rhodocrous* J1 has been observed in three homo-oligomeric structural forms – a dimer, a 480 kDa complex and a variable length, regular helix. Our results confirm that the dimeric species is inactive. We interpret the 'c'-shaped, 480-kDa complexes as being short spirals with fewer than one complete turn. These can be correlated with previously observed active oligomers that occur in the presence of benzonitrile, on heat treatment or on the addition of ammonium sulfate or organic solvent [16–18]. It is interesting that the active 480-kDa complex formed readily from the recombinant enzyme but was not isolated from the native organism [16]. However, a substantially higher salt concentration was used by us and our result is therefore consistent with previously reported association results.

The helical filaments we describe have not been reported previously for nitrilase from *R. rhodochrous* J1. However, cyanide dihydratase from *B. pumilus* is known to form helices under certain pH conditions [4], but the helical parameters of this protein have never been reported. The 3D stain envelope can be interpreted in a way that is consistent with our previous work on cyanide dihydratase from *P. stutzeri*. The common features are the location of the C-terminal region and the sequence insertions (relative to the crystallographically determined homologues) of the nitrilase.

The location of the C-terminal region on the inside of the helix immediately suggests a reason for the failure of the wild-type enzyme to form the long helices. Namely, that steric hindrance resulting from the C-terminal 39 amino acids prevents completion of the turn and formation of the D surface. Our observation that constructs on either side of the experimentally observed cleavage at approximately residue 327 do not form stable long helices suggests that the truncation at residue 327 is the 'optimal point' for cleavage, producing a homogeneous population of long helices of the nitrilase. At this position, the packing results in the putative D surface salt bridges being optimally aligned and the helix elongates readily, whereas on either side of this optimum the packing is too tight or too loose, resulting in unstable, short helices.

Vacant density in the reconstruction corresponds in location and volume to the 28 residues per dimer omitted from the model at the C-terminus and the 68 residues per dimer at the C surface. The sequence insertions and C-terminal extension also occur in the cyanide dihydratases and cyanide hydratases [12], indeed these features are common to a large number of the microbial nitrilases. The location of the sequence insertions implicates at least some of these residues in the C surface interactions and points to them being necessary for helix or spiral formation. This, in turn, implicates structural changes resulting from this interaction in the activation of the enzyme that occurs on oligomerization.

An open question is the reason for the cleavage at position 326 or 327. We cannot rule out the presence of a contaminating proteinase arising from the *E. coli*, but this seems unlikely given the specificity of the cut, that the only known proteinases likely to cut at either of these locations have a very broad specificity, and that no further degradation takes place over a period exceeding 1 year. We therefore suggest that this is an autolysis. The residues responsible for the cleavage remain unknown.

The biological role of nitrilases is suggested to be the metabolism of cyanosugars, hormone precursors containing nitriles and other organocyanide compounds produced by prokaryotes and eukaryotes [4]. Several specific gene clusters containing the nitrilase gene have been identified in both cultured bacteria and environmentally sampled DNA [5]. If we postulate that the tendency to form spirals or helices is widespread in nitrilases, then a possible role for the helices could be to act as a scaffold for proteins expressed by genes in the cluster, leading to an organelle-like assembly. Assembly of dimers following post-translational cleavage into an enzymatically active complex suggests a regulatory mechanism. This presumably occurs in the cells in addition to the transcriptional regulation described previously [22]. This multistep process leads to a concentration of the active sites the role of which could be to protect the organism from harmful nitriles.

Even though the functional significance *in vivo* is unknown, biotechnological applications of artificially made helices are suggested. The long helices provide a concentration of active sites that can easily be purified, immobilized and stored for long periods.

In conclusion, we have discovered how to produce active, long helical oligomers of the nitrilase from *R. rhodochrous* J1. We have identified surfaces involved in forming and maintaining the helix, and suggest that oligomerization utilizing these or similar interactions may be common among microbial nitrilases, cyanide dihydratases and cyanide hydratases. The active *R. rhodochrous* J1 nitrilase helix has a 4.9-fold screw axis, which would preclude the formation of three dimensional crystals. Although crystallization and X-ray structure determination of this enzyme remains elusive, strategies for preventing helix formation by mutating the residues involved in helix stabilization are suggested by this study. High-resolution structure determination will provide more insight into the configuration of the active site, the link between oligomerization and activity, as well as an understanding of how the versatile chemistry of this enzyme class arises from the Glu, Lys, Cys catalytic triad.

## Experimental procedures

### Expression of recombinant *R. rhodochrous* J1 nitrilase

Recombinant nitrilase from *R. rhodochrous* J1 was expressed in *E. coli* strain BL21 (DE3) pLysS cells carrying plasmid pET30a (Novagen, Madison, WI), in which the gene for the wild-type enzyme was incorporated. Mutant J1ΔC327 was recombinantly expressed using pET29b, and J1ΔC302, J1ΔC311, J1ΔC317 and J1ΔC340 were expressed using pET26b, all in the same *E. coli* strain. A small amount of transformed host cells was used to inoculate 5 mL of Luria–Bertani broth containing 25 $\mu g \cdot mL^{-1}$ kanamycin and 200 $\mu g \cdot mL^{-1}$ chloramphenicol. This was grown overnight and then diluted into 1 L of Luria–Bertani broth containing 25 $\mu g \cdot mL^{-1}$ kanamycin and grown at 37 °C. When cells reached an $D_{600}$ of $\sim 1$, isopropyl-β-D-thiogalactopyranoside was added to a final concentration of 1 mM to induce protein expression. Cells were grown overnight, pelleted (4000 ***g***, 10 min, 4 °C) and resuspended in 40 mL of 100 mM $KH_2PO_4$ pH 7.8 (buffer A) containing one tablet of protease cocktail inhibitors (Roche Diagnostics

GmbH, Mannheim, Germany). Cells were disrupted using a Misonix® 3000, sonicator (Misonix Inc., Farmingdale, NY) with pauses for cooling, for a total of 4 min and then harvested by centrifugation (20 000 ***g***, 4 °C, 30 min). The supernatant was filtered through a 0.45 μm Millipore membrane and then applied to an anion-exchange column (Q-Sepharose XK 26/20; Amersham Biosciences, Piscataway, NJ) previously equilibrated with 100 mM $KH_2PO_4$, 200 mM KCl, 10% (v/v) ethanol, pH 7.8 (the J1ΔC327 was subjected to 30–40% ammonium sulfate precipitation prior to this step). The protein was eluted using 100 mM $KH_2PO_4$, 400 mM KCl, 10% (v/v) ethanol, pH 7.8, whereas the J1ΔC327 mutant was eluted using a linear gradient from 0.1 to 1 M KCl in the same buffer. Active peak fractions were analysed by reducing SDS/PAGE. Protein concentration was determined using either Bradford assay or photometrically at $\lambda = 280$ nm using the known extinction coefficient of *R. rhodochrous* J1 nitrilase [15] of 0.93 $mg^{-1}{\cdot}cm^{-1}{\cdot}mL^{-1}$. Active fractions were pooled and concentrated to 8.5 $mg{\cdot}mL^{-1}$ using an Amicon stirred cell (Millipore, Billerica, MA) with a 10 kDa exclusion membrane (Millipore PM10) and ultrafiltration subsequently applied to the gel filtration column (Sephacryl S400 HRXk 16/70; Amersham Biosciences). Proteins were eluted with 100 mM $KH_2PO_4$, 200 mM NaCl, pH 7.8 (buffer B) and where necessary, this step was repeated to rid the protein of contaminating GroEL-like particles. All gel filtration columns were previously calibrated using Bio-Rad standards (supplementary Fig. S1) at the same flow rate. Active peak fractions were separated on reducing SDS/PAGE and bands visualized by silver staining. An active sample of 1-month-old purified enzyme kept refrigerated at 4 °C was filtered through a 0.22 μm membrane and applied to gel filtration (TSK G5000$PW_{XL}$ column; Tosoh Bioscience, GmbH, Stuttgart, Germany) previously equilibrated and eluted using buffer B. At the end of each chromatographic step, the active protein was investigated by negative-stain electron microscopy.

## Assay for enzyme activity

Nitrilase activity was analysed by assaying the release of ammonia as described previously [23]. Reactions were carried out in 1 mL volumes containing 2 μL of enzyme solution, 988 μL of buffer A and 10 μL of 100 mM benzonitrile (dissolved in 1 mL ethanol to increase its solubility). The reaction was allowed to occur for 1 h at room temperature followed by the addition of 40 μL phenol–alcohol, 40 μL sodium nitroprusside and 100 μL of freshly prepared oxidizing solution [1 part NaOCl to 4 parts alkaline complexing agent (10 g sodium citrate, 0.5 g sodium hydroxide made up to 50 mL with distilled water)]. Reaction mixtures were incubated for 1 h at room temperature and the colour change was recorded by measuring the absorbance at 620 nm. One unit of the enzyme was defined as the amount that converts 1 μmole of benzonitrile in 1 min to produce an equivalent amount of benzoate and ammonia. Every second fraction eluted from the columns was assayed for activity.

## Negative-stain electron microscopy

Four microlitres of purified enzyme solution was pippetted onto a fresh glow-discharged grid previously coated with a thin carbon support film under vacuum. In order to reduce precipitation between phosphate buffer and uranyl acetate, grids were subjected to two successive water washes followed by staining with 2% uranyl acetate. At each step, excess sample, wash and stain were blotted. Grids were air-dried before electron microscopy. The salt concentration in the buffer was reduced by a 5–10-fold dilution with distilled water. All staining was carried out at room temperature. Micrographs for image processing were recorded slightly under focus on Kodak S0163 film under low-dose conditions on a JEOL 1200EX II transmission electron microscope operating at 120 kV.

## Image processing

Good-quality negatives were scanned using a Leafscan™ 45 scanner at pixel size of 10 μm, giving 2 Å per pixel at the specimen level. The oligomeric particles were extracted in $160 \times 160$ pixel boxes and later binned by a factor of two. Raw images ($\sim$ 11 000) were band-pass filtered (20 to 1.5 nm) and masked and then iteratively aligned and classified using routines in the SPIDER program suite [24]. A 3D reconstruction of the oligomeric state was not pursued because of sample heterogeneity. Filament segments (13 506) were windowed in $256 \times 256$ pixel boxes using boxer, a program from the EMAN package [25], and then binned by a factor of two. The overlap between boxes along the length of a single filament was 96%. 3D reconstruction was carried out using the iterative helical real space reconstruction method [19]. The reconstruction was based on 13 506 segments, each 12.8 nm long. After several cycles of iteration, the twofold axis perpendicular to the helix axis, which corresponded to the dyad axis of the dimer, became readily apparent and twofold symmetry was imposed on the reconstruction in subsequent cycles. The reconstruction was low-pass filtered to 1.8 nm and visualized using UCSF CHIMERA [26].

## Homology modelling and docking

The search for structural homologues and sequence alignment was done using MGENTHREADER [20]. Pair-wise alignment of the solved structures was done using ALIGN [27]. Based on the alignment (slightly modified by hand), a 3D model of the J1 nitrilase dimer having 313 residues (of

366 due to lack of a template for its extended C-terminus) was constructed using MODELLER [28]. Side-chain orientation was optimized using SCWRL [29]. The model was evaluated using PROCHECK [30] and PROSA [31] and visualized with PYMOL [32]. Automatic fitting of a helix model comprising two turns made up of nine dimers of the J1 nitrilase model without the insertions or the C-terminal extension, was carried out using the contour-based low-resolution (COLORES) program implemented in the SITUS package [21]. The nine-dimer helix model was generated by applying the helical symmetry operators to a single dimer model whose twofold axis was located on the *x*-axis. Once the helical parameters were determined, the dihedral ($D_1$) symmetry of the helix allows only two additional degrees of freedom for fitting such a model, namely the azimuthal rotation about the *x*-axis and translation along the same axis. All surface renderings were carried using UCSF CHIMERA [26].

### N-Terminal sequencing and mass spectrometry

Following results from gel filtration and reducing SDS/PAGE, a purified 1-month-old sample (0.75 $mg \cdot mL^{-1}$) of the nitrilase was sent to Commonwealth Biotechnologies, Inc. (Richmond, Virginia) for N-terminal sequencing and MALDI-TOF MS. One hundred microlitres of sample was subjected to 10 cycles of Edman degradation to determine the amino acid sequence. For MS, 1 μL of undiluted sample was mixed with 1 μL of matrix (ferulic acid) and then spotted onto a sample plate. The sample was desalted to improve the signal.

## Acknowledgements

We thank Professor Charles Brenner for the generous gift of the recombinant expression plasmid, Professor Edward H. Egelman for his assistance with the iterative helical real-space reconstruction programs, Dr Dean Brady for access to the HPLC equipment at CSIR Bio/Chemtek and Professor Michael Benedik for his comments on the manuscript. We greatly appreciate the substantial support we have received from the Carnegie Corporation of New York. RNT was funded by an international scholarship from UCT as well as a studentship from CSIR (Bio/Chemtek).

## References

1 Pace H & Brenner C (2001) The nitrilase superfamily: classification, structure and function. *Genome Biol* **2**, 1–9.
2 O'Reilly C & Turner PD (2003) The nitrilase family of CN hydrolyzing enzymes – a comparative study. *J Appl Microbiol* **95**, 1161–1174.
3 Banerjee A, Sharma R & Banerjee UC (2002) The nitrile-degrading enzymes: current status and future prospects. *Appl Microbiol Biotechnol* **60**, 30–44.
4 Robertson DE, Chaplin JA, DeSantis G, Podar M, Madden M, Chi E, Richardson T, Milan A, Miller M, Weiner DP *et al.* (2004) Exploring nitrilase sequence space for enantioselective catalysis. *Appl Environ Microbiol* **70**, 2429–2436.
5 Podar M, Eads JR & Richardson TH (2005) Evolution of a microbial nitrilase gene family: a comparative and environmental genomics study. *BMC Evol Biol* **5**, 1–13.
6 Pace HC, Hodawadekar SC, Draganescu A, Huang J, Bieganowski P, Pekarsky Y, Croce CM & Brenner C (2000) Crystal structure of the worm NitFhit Rosetta Stone protein reveals a Nit tetramer binding two Fhit dimers. *Curr Biol* **10**, 907–917.
7 Nakai T, Hasegawa T, Yamashita E, Yamamoto M, Kumasaka T, Ueki T, Nanba H, Ikenaka Y, Takahashi S, Sato M *et al.* (2000) Crystal structure of *N*-carbamyl-D-amino acid amidohydrolase with a novel catalytic framework common to amidohydrolases. *Structure* **8**, 729–737.
8 Hashimoto H, Aoki M, Shimizu T, Nakai T, Morikawa H, Ikenaka Y, Takahashi S & Sato M (2004) *Crystal Structure of C171A/V236A Mutant of* N-*Carbamyl-D-Amino Acid Amidohydrolase*. RCSB Protein Databank (1uf5).
9 Kumaran D, Eswaramoorthy S, Gerchman SE, Kycia H, Studier FW & Swaminathan S (2003) Crystal structure of putative CN hydrolase from yeast. *Proteins: Struct Funct Genet* **52**, 283–291.
10 Sakai N, Tajika Y, Yao M, Watanabe N & Tanaka I (2004) Crystal structure of hypothetical protein PH0642 from *Pyrococcus horikoshii* at 1.6 Å resolution. *Proteins: Struct Funct Bioinform* **57**, 869–873.
11 Agarkar VB, Kimani SW, Cowan DA, Sayed MF-R & Sewell BT (2006) The quaternary structure of the amidase from *Geobacillus pallidus* RAPc8 is revealed by its crystal packing. *Acta Crystallogr* **F62**, 1174–1178.
12 Sewell BT, Thuku RN, Zhang X & Benedik MJ (2005) The oligomeric structure of nitrilases: the effect of mutating interfacial residues on activity. *Ann NY Acad Sci* **1056**, 153–159.
13 Sewell BT, Berman MN, Meyers PR, Jandhyala D & Benedik MJ (2003) The cyanide degrading nitrilase from *Pseudomonas stutzeri* AK61 is a two-fold symmetric, 14-subunit spiral. *Structure* **11**, 1–20.
14 Jandhyala D, Berman M, Meyers PR, Sewell BT, Willson RC & Benedik MJ (2003) Cyn D, the cyanide dihydratase from *Bacillus pumillus*: gene cloning and structural studies. *Appl Environ Microbiol* **69**, 4794–4805.
15 Kobayashi M, Nagasawa T & Yamada H (1989) Nitrilase of *Rhodococcus rhodochrous* J1: purification and characterization. *Eur J Biochem* **182**, 349–356.

16 Nagasawa T, Wieser M, Nakamura T, Iwahara H, Yoshida T & Gekko K (2000) Nitrilase of *Rhodococcus rhodochrous* J1: conversion into the active form by subunit association. *Eur J Biochem* **267**, 138–144.
17 Stevenson DE, Feng R, Dumas F, Groleau D, Mihoc A & Storer AC (1992) Mechanistic and structural studies on *Rhodococcus* ATCC 39484 nitrilase. *Biotechn Appl Biochem* **15**, 283–302.
18 Harper DB (1977) Microbial metabolism of aromatic nitriles: enzymology of C–N cleavage by *Norcadia* sp. (*Rhodochrous* group) NCIB 11216. *Biochem J* **165**, 309–319.
19 Egelman EH (2000) A robust algorithm for the reconstruction of helical filaments using single-particle methods. *Ultramicroscopy* **85**, 225–234.
20 Jones DT (1999) GenTHREADER: an efficient and reliable protein fold recognition method for genomic sequences. *J Mol Biol* **287**, 797–815.
21 Chacon P & Wriggers W (2002) Multi-resolution contour-based fitting of macromolecular structures. *J Mol Biol* **317**, 375–384.
22 Komeda H, Hori Y, Kobayashi M & Shimizu S (1996) Transcriptional regulation of the *Rhodococcus rhodochrous* J1 *nit*A gene enconding a nitrilase. *Proc Natl Acad Sci USA* **93**, 10572–10577.
23 Piotrowski M, Schonfelder S & Weiler EW (2001) The *Arabidopsis thaliana* isogene *NIT4* and its orthologs in tobacco encode β-cyano-L-alanine hydratase/nitrilase. *J Biol Chem* **276**, 2616–2621.
24 Frank J, Radermacher M, Penczek P, Zhu J, Li Y, Ladjadj M & Leith A (1996) SPIDER and WEB: processing and visualization of images in 3D electron microscopy and related fields. *J Struct Biol* **116**, 190–199.
25 Ludtke SJ, Baldwin PR & Chiu W (1999) EMAN: semi-automated software for high-resolution single particle reconstructions. *J Struct Biol* **128**, 82–96.
26 Pettersen EF, Goddard TD, Huang CC, Couch GS, Greenblatt DM, Meng EC & Ferrin TE (2004) UCSF Chimera – a visualization system for exploratory research and analysis. *J Comput Chem* **25**, 1605–1612.
27 Cohen GH (1997) ALIGN: a program to superimpose protein coordinates, accounting for insertions and deletions. *J Appl Crystallogr* **30**, 1160–1161.
28 Sali A & Blundell TL (1993) Comparative protein modeling by satisfaction of spatial restraints. *J Mol Biol* **234**, 779–815.
29 Bower JM, Cohen FE & Dunbrack RL Jr (1997) Prediction of protein side-chain rotamers from a backbone-dependent rotamer library: a new homology modeling tool. *J Mol Biol* **267**, 1268–1282.
30 Laskowski RA, MacArthur MW, Moss DS & Thornton JM (1993) PROCHECK: a program to check the stereochemical quality of protein structures. *J Appl Crystallogr* **26**, 283–291.
31 Sippl M (1993) Recognition of errors in three-dimensional structures of proteins. *Proteins: Struct Funct Genet* **17**, 355–362.
32 DeLano WL (2002) *The PyMOL Molecular Graphics System*. DeLano Scientific, San Carlos, CA. http://www.pymol.org.
33 Makowski L & Caspar DLD (1981) The symmetries of filamentous phage particles. *J Mol Biol* **145**, 611–617.

## Supplementary material

The following supplementary material is available online:

**Fig. S1.** Calibration of the TSK G5000PW$_{XL}$ column used for the elution of 1-month-old *Rhodococcus rhodochrous* J1 (J1 nitrilase).

**Fig. S2.** Convergence of the IHRSR algorithm after 22 cycles.

**Fig. S3.** Cartoon representation of the structural homologues and 3D model of the nitrilase from *Rhodococcus rhodochrous* J1.

This material is available as part of the online article from http://www.blackwell-synergy.com

Please note: Blackwell Publishing is not responsible for the content or functionality of any supplementary material supplied by the authors. Any queries (other than missing material) should be directed to the corresponding author for the article.